

Disturbance-free high-speed sinusoidal phase-modulating laser diode interferometer

Takamasa Suzuki, Toshiyuki Maki, Xuefeng Zhao, and Osami Sasaki

A surface profiler that incorporates a feedback controller to eliminate external disturbances is proposed and demonstrated. Its overall performance is dependent on the frequency response of the feedback loop. The frequency of the modulating signal strongly influences the response of the feedback controller. When we used the integrating-bucket method, the CCD camera had to be operated at a low-frequency video rate. Our technique uses a CCD camera equipped with an electronic shutter. The shutter function enables us to apply high-speed sinusoidal phase modulation to the conventional integrating-bucket method under the standard video rate. © 2002 Optical Society of America

OCIS codes: 120.3180, 120.3940, 120.5050, 120.5060, 120.6660, 140.2020.

1. Introduction

As with any technology, each successive generation of interferometer reveals the shortcomings of its predecessor. Earlier models, which were highly vulnerable to external disturbances that could and often did deteriorate measurement accuracy, have been replaced by feedback-type laser diode (LD) interferometers. The feedback-type interferometers can also be used to measure vibration^{1,2} because they detect minute changes in the interference signal itself when a photodiode (PD) is used as the photodetector. Temporal signals detected by the PD are easily processed. When the LD is not being actively modulated, the interference signal itself can be used as a feedback signal. If the LD is modulated with a continuous signal, however, we extract the feedback signal by using a modulating signal. In this case, the frequency response of the feedback system depends on the modulating frequency used. Not surprisingly, as the modulating signal frequency rises, the quality of the feedback system used to eliminate mechanical disturbances does so as well. This disturbance elimination technique was used in phase-shifting interferometers (PSIs).^{3,4} Surface profiles were measured, not on sophisticated optical benches,

but rather on a simple wooden table in these PSIs. Since the interference signals of PSIs are modulated by step-type signals, the static fringe pattern detected by spatial filtering detectors can easily be used as a feedback signal. The PSI, however, requires four fringe images having a phase shift of $(\pi/2)i$ ($i = 0, 1, 2, 3$). It is not so easy to apply a shift of $\pi/2$ precisely at the phase of interference images.

In contrast, the integrating-bucket method⁵ is convenient to use when a CCD camera is used to capture images. We detected the phase by using the four images obtained in a given modulating period. Parameter adjustments are easier to make when we use this method rather than a PSI. The parameters in this case represent the initial phase of the modulating current and the modulation depth that depends on the amplitude of the modulating current.⁶ The modulating frequency is restricted by the National Television System Committee (NTSC) standards when a general-purpose CCD camera is used. In such cases, the frequency response of the feedback signal⁷ extracted from the interference signal is poor. Therefore, equipping the bucket-type interferometer with an adequate feedback control proved to be extremely difficult when we used a general-purpose CCD camera. If we used a special CCD camera with a high frame rate, the restrictions of the NTSC standards would not apply. We would, however, need a special video capture with a sizable memory, which would be costly.

The technique we propose here uses an electronic shutter that enables us to control the charge storage period, which in turn permits the frequency of the

T. Suzuki (takamasa@eng.niigata-u.ac.jp), T. Maki, X. Zhao, and O. Sasaki are with the Faculty of Engineering, Niigata University, 8050 Ikarashi 2, Niigata 950-2181, Japan.

Received 19 June 2001; revised manuscript received 3 October 2001.

0003-6935/02/101949-05\$15.00/0

© 2002 Optical Society of America

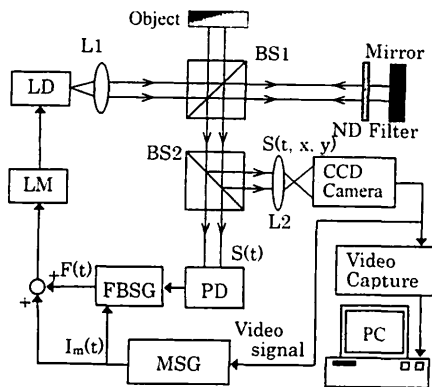


Fig. 1. Setup of the disturbance-free high-speed sinusoidal phase-modulating laser diode interferometer: LM, laser diode modulator; FBSG, feedback-signal generator; MSG, modulating-signal generator; ND filter, neutral density filter.

modulating signal to be increased significantly even if we use a general-purpose CCD camera.

2. Principle

A. Optical Setup

The setup of our interferometer is shown in Fig. 1. The beam that radiates from the LD is collimated by lens L1 and fed into a Twyman-Green interferometer. The interference fringe is then divided by beam splitter BS2. One of these fringes was acquired with a CCD camera as spatiotemporal signal $S(t, x, y)$ and then processed by a computer. The other temporal signal, $S(t)$, which was detected by a PD, was processed by the feedback-signal generator to produce the signal required to eliminate disturbance.

The complex video signal output based on the NTSC standards is fed into the modulating-signal generator. This modulating signal $I_m(t)$ and feedback signal $F(t)$ are injected into the LD through laser diode modulator LM. When we use the sinusoidal signal

$$I_m(t) = m \cos(\omega_c t + \theta) \quad (1)$$

as the modulating signal, the interference signal is then given by⁷

$$S(t, x, y) = a + b \cos[z \cos(\omega_c t + \theta) + \alpha(x, y)], \quad (2)$$

where

$$z = 2\pi m \beta L_0 / \lambda_0^2, \quad (3)$$

$$\alpha(x, y) = 4\pi L(x, y) / \lambda_0 \quad (4)$$

represent the modulation depth and the phase distribution on the test surface, respectively; and z is determined by amplitude m , modulation efficiency β , and optical pass difference L_0 . The profile of the object is represented by $L(x, y)$.

B. Bucket Method

A schematic of the bucket method⁵ is shown in Fig. 2. Images detected by the CCD camera are represented

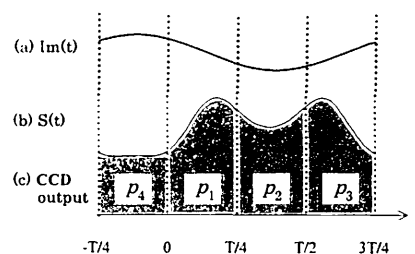


Fig. 2. Schematic of the integrating-bucket method.

by the temporally integrated values of the incident interference signal. We detected four images:

$$p_i(x, y) = \int_{T_c(i-1)}^{T_c i} S(t, x, y) dt \quad (i = 1-4), \quad (5)$$

where $T_c = T/4$ is the charge storage period. T_c is set to a quarter period of the modulating signal in our system. Phase distribution $\alpha(x, y)$ is then given by

$$\alpha(x, y) = \frac{p_1 + p_2 - p_3 - p_4}{p_1 - p_2 + p_3 - p_4}, \quad (6)$$

under the conditions $z = 2.45$ rad and $\theta = 56^\circ$. The previous problem with this method was that the modulating frequency was restricted to a frame rate of 1/30 s.

C. Modification of the Bucket Method

Figure 3 illustrates the method used to increase modulation frequency under NTSC standards. One quarter period of a conventional modulating signal [Fig. 3(a)] is equal to a T_f frame rate of 1/30 s. In other words, the frequency of the modulating signal is restricted to 7.5 Hz under NTSC standards. The technique under discussion [Fig. 3(b)] uses the shutter function of a CCD camera. The integrated signal is cleared once at the rising edge of the shutter pulse, after which a newly integrated signal is read out at the rising edge of the CCD readout pulse. In this case, the quarter period of the modulating signal

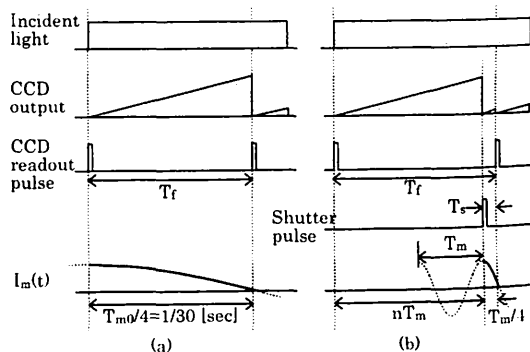


Fig. 3. Schematic of (a) a conventional modulating signal and (b) a high-speed modulating signal.

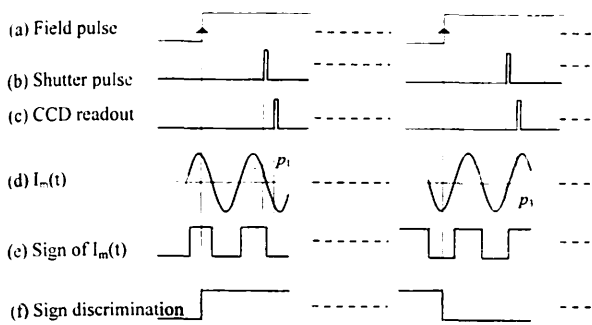


Fig. 4. Timing chart of signal processing for order discrimination.

(T_m), or charge storage period, is equal to the shutter speed (T_s) and is represented by

$$T_m/4 = T_s, \quad (7)$$

which indicates the need for a modulating signal whose frequency ($1/T_m$) is $1/(4T_s)$ Hz. With the bucket method, however, the phase of the modulating signal must be shifted by $\pi/2$ for each integration as shown in Fig. 2. This condition is expressed as

$$T_f = (n \pm 1/4)T_m, \quad (8)$$

where n is an integer. Equations (7) and (8) provide relation

$$n = \text{round} \left[\frac{1}{4} \left(\frac{T_f}{T_s} \mp 1 \right) \right], \quad (9)$$

where $\text{round} [\]$ rounds off the argument. From Eqs. (7), (8), and (9), the actual modulating frequency f_m ($=1/T_m$) is given by

$$f_m = \frac{1}{4T_f} \left\{ 4 \text{round} \left[\frac{1}{4} \left(\frac{T_f}{T_s} \mp 1 \right) \right] \pm 1 \right\}. \quad (10)$$

D. Discrimination of the Order of Images

For the bucket method we must determine the order of the images because order in the calculation is important as shown in Eq. (6). In our experiment we checked the order by observing the light-emitting diode (LED) that lights for a specific period. A schematic of the signal processing for order discrimination is shown in Fig. 4. A comparator detects the sign of the modulating signal as shown in Fig. 4(e). The signals are sampled each time the field pulse rises and signs are discriminated as shown in Fig. 4(f). The discriminated sign observed over eight periods is shown in Fig. 5. Figure 5(c) shows that the sign of the modulating signal changes when the even image is detected. The driving signal for LED shown in Fig. 5(e) is generated by the AND operation of signals shown in Figs. 5(c) and 5(d). We created the signal shown in Fig. 5(d) from the discriminated signal by using a half-divider. When eight successive images were captured with the CCD camera, we found two successive images that were brighter than the other images. The phase distribution was then

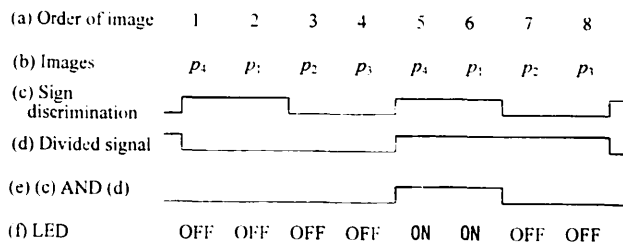


Fig. 5. Discrimination of the order of images.

calculated with four successive images $p_4, p_1, p_2,$ and p_3 that are detected prior to the bright images.

3. Experiment

A. Experimental Setup

In the setup shown in Fig. 1, the wavelength of the LD was 685 nm. The size and number of pixels in the CCD image sensor were $6.35 \mu\text{m} \times 7.40 \mu\text{m}$ and $768(\text{H}) \times 494(\text{V})$, respectively. The converted pixel size on the computer was $4.3 \mu\text{m} \times 4.3 \mu\text{m}$ for the measurement because the image was magnified by L2, and it shrank when the image-capture board was used. Figure 6 shows a block diagram of the modulating-signal generator, which generates the modulating signal from the NTSC video signal. A video sync separator strips the synchronous field signal from the composite video signal. The field signal period is T_f . The phase-locked loop increases the number of cycles of the field signal by N times. A divider was used to divide this frequency-raised pulse by four. This divided pulse, whose period is T_m , was fed to the external trigger input of an oscillator that converts the rectangular pulse to a sinusoidal signal. The phase shifter shifts the phase of this sinusoidal signal by 56° . A bandpass filter was used to eliminate useless harmonics in the sinusoidal signal.

The CCD camera in our experiment has eight selectable shutter speeds: $1/100, 1/250, 1/500, 1/1000, 1/2000, 1/5000, 1/10000,$ and $1/100000$. After selecting the $1/10000$ s shutter speed, we confirmed its acquisition by observing the shutter pulse, which was determined to be $106 \mu\text{s}$. This figure provided the required modulating frequency ($f_{m0} = 1/4T_s$) of 2358.5 Hz. In contrast, the modulation frequency f_m calculated with Eq. (10) was 2361.32 Hz for $n = 78$, which is in approximate agreement with the desired modulation frequency f_{m0} . Modulating signal $I_m(t)$ and a part of the interference signal $S(t)$ detected by the PD are fed into the feedback-signal

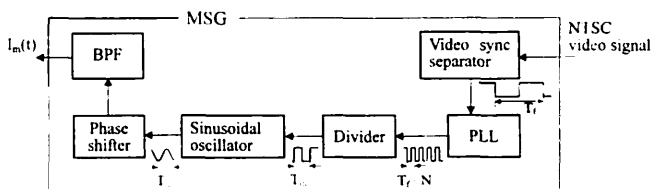


Fig. 6. Block diagram of the modulating-signal generator: PLL, phase-locked loop; BPF, bandpass filter.

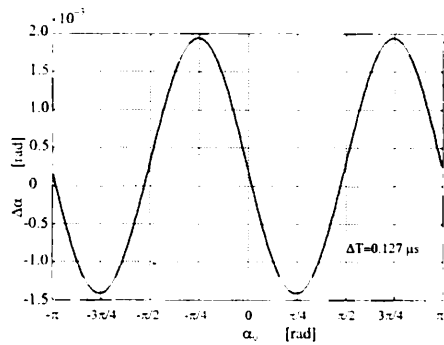


Fig. 7. Calculation of the error caused by the time difference between T_s and $T_m/4$.

generator as shown in Fig. 1 and described in Ref. 7. Two signals, $I_m(t)$ and $S(t)$, are multiplied and the desired feedback signal $F(t)$ is extracted by the low-pass filter. The cutoff frequency of the low-pass filter was $\sim 1/10$ of the modulating frequency to eliminate the carrier component sufficiently. In our system, the cutoff frequency of the low-pass filter was 240 Hz, which is quite high and is sufficient to eliminate external disturbance. The modulating signal is mixed with the feedback signal $F(t)$ and fed into the LD to implement sinusoidal phase modulation and disturbance elimination at the same time.

B. Error Analysis

It is difficult to achieve the exact condition indicated by Eq. (7) because shutter speed T_s is selected discretely for a general-purpose CCD camera. We analyzed the error caused by the time difference ΔT between T_s and $T_m/4$. The ΔT is $0.127 \mu\text{s}$ with respect to the modulation frequency that we used as mentioned above. For error analysis, we calculated Eq. (6) by changing the phase $\alpha(x, y)$, which is the

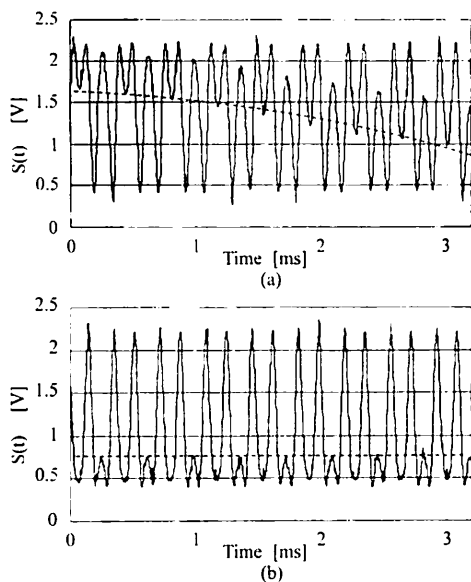


Fig. 8. Interference signals observed by the photodiode (a) without and (b) with feedback control.

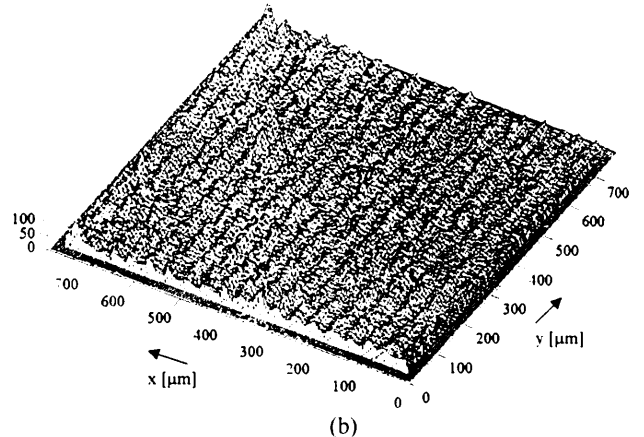
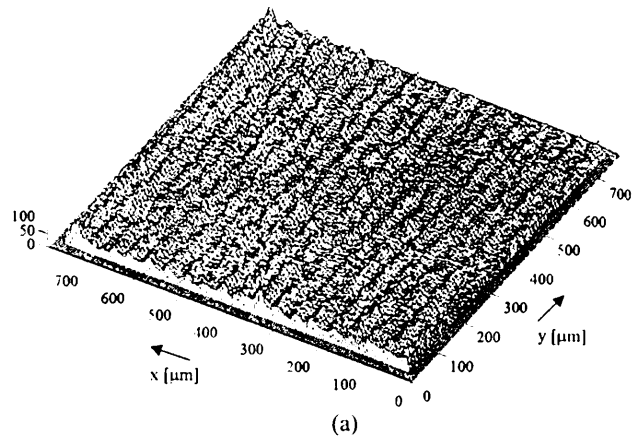


Fig. 9. Three-dimensional surface profile of a diamond-turned aluminum disk.

phase distribution in Eq. (2). We assume that coordinates x and y are fixed. Therefore, for this calculation, $\alpha(x, y) = \alpha_0$ does not depend on x and y . The phase error denoted by $\Delta\alpha = \alpha_0 - \alpha_m$ is shown in Fig. 7, where α_m is the phase calculated by the actual charge storage period $T_m/4$. According to Fig. 7, the maximum error is 1.95×10^{-3} rad, which corresponds to a distance of 0.1 nm. This error is small enough to be used to perform surface-profile measurements.

C. Results

We measured interference as well as the surface profile of a diamond-turned aluminum disk. These measurements were not implemented by use of any dedicated optical benches, but simply fixed to a horizontal surface, which in this case was a 5-mm-thick iron plate on a wooden desk. Interference signals detected with the PD are shown in Fig. 8. The dashed curves indicate the phase variations. When the feedback control was turned off, undesirable phase changes induced by external disturbances were superimposed upon $S(t)$ as shown in Fig. 8(a). Such phase changes were completely eliminated in $S(t)$ when observed during feedback control as shown in Fig. 8(b).

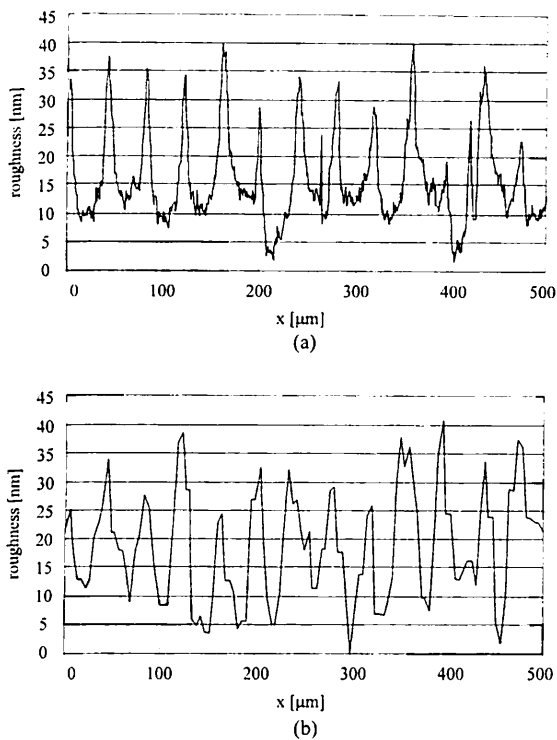


Fig. 10. Two-dimensional surface profiles of a diamond-turned aluminum disk measured with (a) a Talystep profilometer and (b) our system.

Surface-profile measurements were demonstrated with the feedback control. Figure 9 provides the three-dimensional surface profile of the diamond-turned aluminum disk with a 35- μm cutting pitch. The second measurement shown in Fig. 9(b) was implemented 10 min after the first measurement shown in Fig. 9(a). Repeatability is estimated as 4.2-nm rms for these measurements. We believe that the error is the result of mechanical displacement and change in room temperature.

Two-dimensional profiles traced along the x direction of the disk are shown in Fig. 10. Figures 10(a)

and 10(b) show the results of measurements taken with a Talystep profilometer and with our system, respectively. Although the measured points differ, good agreement exists between the roughness and the cutting pitch along the x direction.

4. Conclusions

We have proposed a feedback-based integrating-bucket method that eliminates external disturbances without any special CCD cameras. The shutter function of the CCD camera enables us to apply high-speed sinusoidal phase modulation, which results in excellent feedback control, to the conventional integrating-bucket method. The measurement results that we obtained on an ordinary horizontal surface indicate that external disturbance is eliminated, while the surface-profile measurement is performed accurately at the same time.

References

1. T. Yoshino, M. Nara, S. Mnatzakanian, B. S. Lee, and T. C. Strand, "Laser diode feedback interferometer for stabilization and displacement measurements," *Appl. Opt.* **26**, 892-897 (1987).
2. T. Suzuki, T. Okada, O. Sasaki, and T. Maruyama, "Real-time vibration measurement using a feedback type of laser diode interferometer with an optical fiber," *Opt. Eng.* **36**, 2496-2502 (1997).
3. J. Liu, I. Yamaguchi, J. Kato, and T. Nakajima, "Active phase-shifting interferometer using current modulation of a laser diode," *Opt. Rev.* **3**, 287-292 (1996).
4. I. Yamaguchi, J. Liu, and J. Kato, "Active phase-shifting interferometers for shape and deformation measurements," *Opt. Eng.* **35**, 2930-2937 (1996).
5. O. Sasaki, H. Okazaki, and M. Sakai, "Sinusoidal phase modulating interferometer using the integrating-bucket method," *Appl. Opt.* **26**, 1089-1093 (1987).
6. T. Suzuki, O. Sasaki, J. Kaneda, and T. Maruyama, "Real-time two-dimensional surface profile measurement in sinusoidal phase modulating laser diode interferometer," *Opt. Eng.* **33**, 2754-2759 (1994).
7. O. Sasaki, K. Takahashi, and T. Suzuki, "Sinusoidal phase modulating laser diode interferometer with a feedback control system to eliminate external disturbance," *Opt. Eng.* **29**, 1511-1515 (1990).